# Inter- and Intramolecular Hydrogen Bonding in Phenol Derivatives: A Model System for Poly-L-tyrosine

**Neil T. Hunt, Andrew R. Turner, and Klaas Wynne***

*Department of Physics, University of Strathclyde, John Anderson Building, 107 Rottenrow East, Glasgow G4 0NG, Scotland, United Kingdom*

*Received: June 3, 2005; In Final Form: August 10, 2005*

The ultrafast dynamics of solutions of phenol and two phenol derivatives—hydroquinone (1,4-benzenediol) and pyrocatechol (1,2-benzenediol)—have been studied with Optically Heterodyne-Detected Optical Kerr-Effect (OHD-OKE) spectroscopy. The solvents, methanol and acetonitrile, were selected to provide strong and weak solvent−solute hydrogen-bonding interactions, respectively, while pyrocatechol features an intramolecular hydrogen bond. Together these provide a series of model systems for polypeptides such as polytyrosine, which facilitate the direct study of inter- and intramolecular hydrogen bonding. A broad contribution to the Raman spectral density of the methanol solutions at frequencies between 150 and 300 $cm^{-1}$ has been observed that is absent in acetonitrile. This contribution has been assigned to solvent−solute hydrogen-bond stretching vibrations. The OHD-OKE response of poly-L-tyrosine has been measured and was found to contain a similar contribution. Density functional theory geometry optimizations and normal mode calculations have been performed using the B3LYP hybrid functional and 6-311++G** basis set. These have yielded a complete assignment of the low-frequency Raman and far-infrared spectra of pyrocatechol for the first time, which has provided information on the nature of the intramolecular hydrogen bond of pyrocatechol.

## I. Introduction

Hydrogen bonding in liquids plays an important role in the structure and chemistry of biomolecules. From stabilizing of biopolymer molecules into structures such as the α-helix or β-sheet to the reversible bond formation that allows the action of enzymes, the hydrogen bond is central to all biological processes. Understanding the dynamics of these interactions is therefore crucial to our exploitation of such systems. Despite much study, however, this understanding remains incomplete.

Studies of intermolecular hydrogen bonding in the gas phase have been performed with clusters of the form phenol(water)$_n$,[1] phenol(methanol)$_n$,[2] and phenol(ammonia)$_n$[3,4] in supersonic jet expansions. These experiments, which employed resonance enhanced multiphoton ionization (REMPI) techniques, showed, for small $n$, a range of narrow transitions in the 0−250 $cm^{-1}$ spectral region that were assigned to vibrational modes involving the intermolecular hydrogen bond of the clusters.

While such studies are useful in determining the frequencies of modes attributable to hydrogen bonds, they cannot fully replicate the behavior of such modes in the liquid phase where all biological processes take place. Furthermore, the presence of a solvent background and transitions due to the backbone of large, complex biomolecules often make the direct spectroscopic observation of hydrogen-bond vibrations problematic. As a result, many studies have been made of hydrogen bonds indirectly via the effect of changes in hydrogen-bonding interactions upon the O−H or O−D stretching modes of solute molecules in water.[5−12]

One exception to this is the 1967 study of Ginn and Wood,[13] which used far-infrared spectroscopy to observe hydrogen-bond stretching vibrations of liquid-phase complexes of phenol with trimethylamine, triethylamine, and pyridine. Transitions were observed in the 120−150 $cm^{-1}$ region. In addition, there are several theoretical studies on a wide range of hydrogen-bonded systems.[14−16]

The aim of this study is to determine directly the contribution of hydrogen bonding to the ultrafast dynamics and low-frequency Raman spectrum of the polypeptide poly-L-tyrosine. This is achieved through the use of model systems featuring a range of phenol derivatives: phenol, hydroquinone (1,4-benzenediol), and pyrocatechol (1,2- benzenediol) (see Chart 1) dissolved in the two solvents methanol and acetonitrile. The phenolic side group of the tyrosine molecule makes these an obvious choice of model system. The solvents have been chosen to provide strong and weak hydrogen-bonding interactions with the solute molecules, respectively, while avoiding the broad low-frequency absorptions that hinder aqueous studies.

The technique used is Optically Heterodyne Detected-Optical Kerr Effect (OHD-OKE) spectroscopy.[17−27] This method has been used extensively to study the dynamics of pure liquids and binary mixtures[28−30] and is increasingly being employed in investigations of more complex liquid-phase systems. Examples of the latter include microemulsions,[31−34] sol−gel confined liquids,[35−38] and of direct relevance to this study liquid crystals,[39−42] polymers,[43−45] biopolymers, and proteins.[46,47] In particular, Giraud et al.[47] studied a range of samples including di-L-alanine, poly-L-alanine, and four globular proteins to determine the effect of local structure on the low-frequency vibrational modes of these molecules. To date, however, no direct experimental study of the spectroscopy of hydrogen bonding in a biologically relevant liquid-phase system exists.

In addition to intermolecular hydrogen bonding, pyrocatechol is thought to feature an intramolecular hydrogen bond, which will enable the study of the effect of these interactions on the low-frequency modes of the molecule in question. To this end,

10.1021/jp052964o CCC: $30.25 
Published on Web 09/17/2005

**CHART 1: Equilibrium Structures of Phenol, Hydroquinone, and Pyrocatechol Calculated with DFT (see text)**

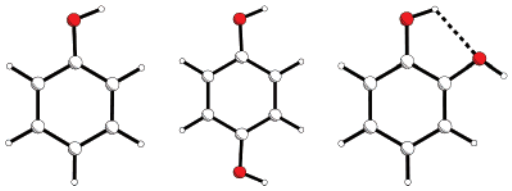

the spectroscopic investigation has been augmented by the use of density functional theory (DFT) calculations of the equilibrium structure and vibrational modes of the phenol derivatives. This is particularly relevant as, despite much study,[48−52] there remains some confusion over the assignment of the low-frequency modes of the hydroxybenzenes, in particular that of pyrocatechol.

The remainder of this paper is organized as follows: section II deals with the experimental and theoretical methods employed while section III relates the results of the study and analysis of the data recovered. These are discussed in section IV and conclusions are drawn in section V.

## II. Experimental Section

**a. OHD-OKE Experiments.** The OHD-OKE setup employed in this work has been described elsewhere.[53] The ultrafast light source is a Kerr-lens mode-locked titanium−sapphire laser operating at 800 nm with a bandwidth of 35 nm and repetition rate of 80 MHz. The pulse duration, measured by second-order autocorrelation at the sample position, was <30 fs. Because of the low solubility of poly-L-tyrosine, some improvements to the spectrometer were necessary to improve sensitivity and signal-to-noise ratio. These include the use of dielectric mirrors to increase laser power at the sample position in conjunction with achromatic lenses to improve the quality of the beam focus. In total, the S:N improvement was in the region of an order of magnitude.

All chemicals have been purchased from Sigma-Aldrich (purity >99%) and used without further purification. All samples have been filtered with 0.2-$\mu$m filters (Millipore) to remove dust and allowed to equilibrate for 24 h at the laboratory temperature prior to use. Pyrocatechol is somewhat light sensitive and therefore all samples containing it were stored in the dark as far as possible to prevent degradation. Each of the three phenol derivatives were dissolved to 1 M concentration in methanol and acetonitrile. In addition, the OHD-OKE responses of samples of 1 M hydroquinone with 0.5, 1, and 2 M methanol dissolved in acetonitrile were also recorded to establish the concentration dependence of any observed methanol-related effects.

To characterize the samples further, mid- and far-infrared spectra have been recorded with a FTIR spectrometer (Bruker Vertex 70).

**b. DFT Calculations.** All DFT calculations have been performed with the Gaussian 03[54] suite of computational chemistry programs. Gas-phase DFT geometry optimizations have been performed for each phenol derivative with use of the B3LYP hybrid functional and the 6-311++G** basis set. For all of the molecules, the starting point for the optimizations was a geometry with no symmetry. This allowed the molecule to relax to the global minimum with no externally imposed symmetry constraints. The optimized structures were then used as the basis for vibrational normal-mode calculations (DFT/B3LYP/6-311++G**), which also included the generation of infrared absorption and Raman scattering intensities.

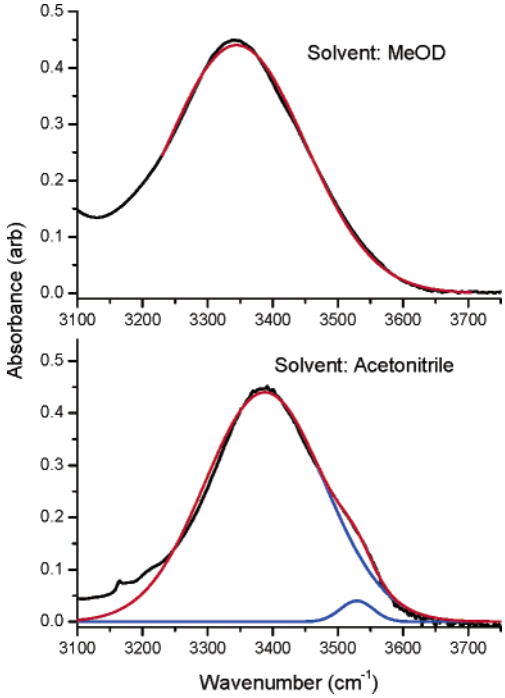


**Figure 1.** Pyrocatechol FTIR data (black line) and fits to Gaussian absorption profiles (red line). The individual components of the fit are also shown (blue line).

## III. Results

**a. FTIR Spectra.** The mid-infrared absorption spectra of all 1 M samples dissolved in deuterated methanol (MeOD) and acetonitrile have been recorded in the O−H stretching region. MeOD was chosen as a solvent for the FTIR studies to prevent the hydroxyl group stretch of the phenol derivatives being obscured by that of the solvent. As an example, Figure 1 displays the spectra of the pyrocatechol samples.

Qualitatively, the hydroxyl-stretching band of all samples is broadened and red-shifted when dissolved in MeOD as opposed to when acetonitrile is the solvent. These effects are characteristic of increased solvent−solute hydrogen bonding in methanol as would be expected. The spectra of the acetonitrile samples show an additional absorption band to the blue side of the main O−H stretching band. By analogy with previous studies of phenol dissolved in the non-hydrogen-bonding solvent chloroform[12] this can be assigned to non-hydrogen-bonded phenol molecules. While it is to be expected that some exchange will occur between the deuterated solvent and the solute, only the O−H stretching band of the solute is of relevance here and it is clear that any exchange is sufficiently slow as to allow this observation to be made.

The FTIR spectra in this region can be examined more quantitatively by fitting Gaussian profiles to the recorded absorption bands. The fit results for all six 1 M samples are presented in Table 1 with examples shown in Figure 1. For all three phenol derivatives dissolved in MeOD, the O−H absorption profile can be fit well by a single Gaussian line shape with a band center close to 3340 $cm^{-1}$ and a width of ~250 $cm^{-1}$. In contrast, when acetonitrile is used, a second Gaussian line shape is required for a good fit. This second band is centered near 3550 $cm^{-1}$ with a width of ~60 $cm^{-1}$. The main line shape is centered near 3400 $cm^{-1}$ with a width of 150 $cm^{-1}$ in the phenol and hydroquinone samples and 216 $cm^{-1}$ when the solute

**TABLE 1: Results of Fitting the Mid-Infrared Spectra in the O−H Stretching Region to Gaussian Profiles as Defined in Eq 4**

| sample | $a_1$ | $\omega_1$ ($cm^{-1}$) | $\sigma_1$ ($cm^{-1}$) | $a_2$ | $\omega_2$ ($cm^{-1}$) | $\sigma_2$ ($cm^{-1}$) |
|---|---|---|---|---|---|---|
| methanol-*d* | | | | | | |
| phenol | 0.357 | 3346.3 | 246.5 | - | - | - |
| hydroquinone | 0.72 | 3340.0 | 261.1 | - | - | - |
| catechol | 0.70 | 3338.7 | 267.2 | - | - | - |
| acetonitrile | | | | | | |
| phenol | 0.37 | 3400.7 | 149.3 | 0.02 | 3548.3 | 65.4 |
| hydroquinone | 0.48 | 3414.9 | 155.0 | 0.03 | 3567.2 | 63.1 |
| catechol | 0.44 | 3387.8 | 216.2 | 0.04 | 3528.9 | 59.9 |

is pyrocatechol. In each case, the area of the lower frequency Gaussian profile was found to be a factor of 40 ± 1 greater than the high-frequency component.

These results confirm the qualitative assessment of the FTIR spectra and provide evidence that the solvent−solute hydrogen-bonding interactions in methanol are stronger than those in acetonitrile because the main O−H stretching absorption band of the hydrogen-bonded solute molecules occurs at lower frequency in methanol.[55] There is also evidence of non-H-bonded phenol groups in acetonitrile via the smaller, high-frequency band observed in these samples. The narrower profile of which further supports this latter assignment. Furthermore, the lower frequency band of pyrocatechol in acetonitrile is different from that of phenol and hydroquinone, being slightly red-shifted and ~40% broader. This can be interpreted as the effect of intramolecular hydrogen bonding between adjacent hydroxyl groups, which is not present in the other two derivatives. That this difference does not manifest itself so strongly in the methanol samples may suggest that pyrocatechol H-bonds preferentially to the solvent in this case.

**b. OHD-OKE Results: Time Domain.** The OHD-OKE responses of the samples studied are presented in Figures 2 and 3. On short time scales (<2 ps, Figure 2) each sample displays a sharp spike near zero delay between the pump and probe pulses. This is due to the electronic hyperpolarizability of the samples and yields no dynamical information. The fact that this is significantly larger for acetonitrile samples is because the solvent possesses a larger polarizability than that of methanol and hence gives a greater response. To quantify this, the 1 M samples contain a solvent:solute molecular ratio of 25:1 in methanol and 20:1 in acetonitrile. Even under these conditions, the response of methanol is significantly smaller than that of the solutes, the large response of the latter originating from the benzene ring. In the case of the acetonitrile solutions, the solute response is also clearly visible, despite the solvent giving a much larger signal than that of methanol.

At pump−probe delays of between 50 and 300 fs, each sample shows a strong shoulder that can be attributed[30] to nuclear dynamics, specifically to librational motion. All samples exhibit an oscillatory component to their OHD-OKE response due to under-damped vibration of intramolecular vibrational modes. Those due to the phenol derivatives are more clearly seen in the methanol samples where the solvent response is negligible while in acetonitrile they are somewhat obscured by the large-amplitude oscillation due to the solvent.

As these samples are solutions, it can be instructive to separate the responses from the solvent and solute (though it should be noted that in the case of strong solvent−solute interactions this procedure may become invalid). In the case of methanol, the solvent response is small in comparison to that of the solute though this is not the case for acetonitrile. Both subtraction of the solvent response and further analysis are facilitated by Fourier transformation of the data into the frequency domain (see below).

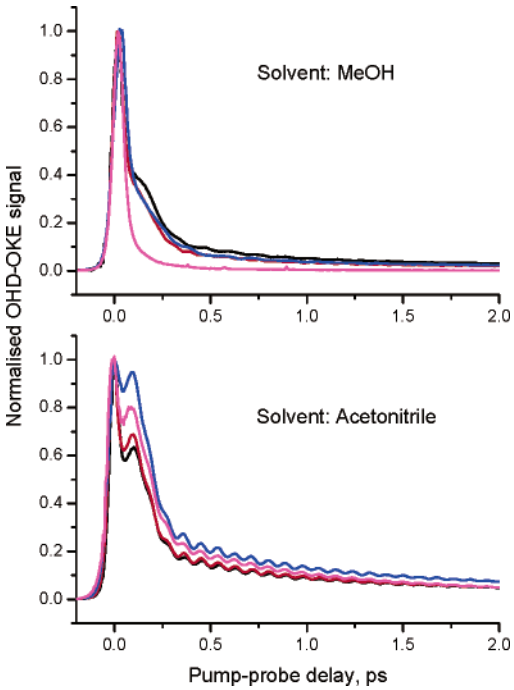


**Figure 2.** OHD-OKE data for 1 M solutions of phenol (black), hydroquinone (red), and pyrocatechol (blue) in methanol and acetonitrile. Data for the neat solvents (pink) are also shown. All data have been normalized to the signal at zero pump−probe delay.

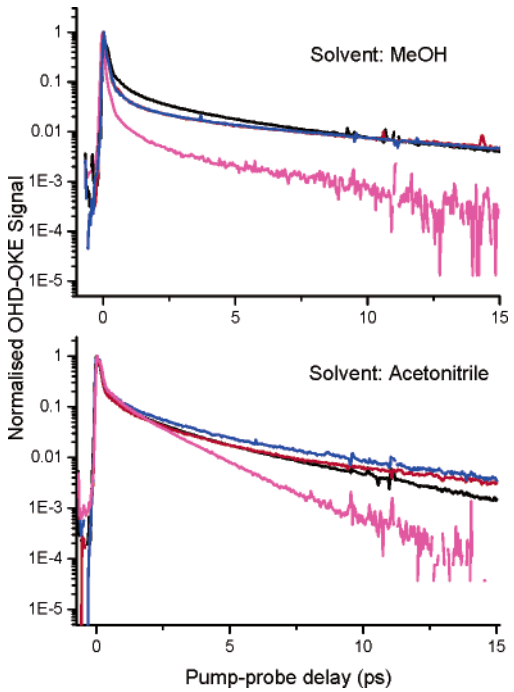


**Figure 3.** Semilogarithmic plots of OHD-OKE data for 1 M solutions of phenol (black), hydroquinone (red), and pyrocatechol (blue) in methanol and acetonitrile. Data for the neat solvents (pink) are also shown.

When studied over longer time scales (Figure 3), the OHD-OKE responses reveal a slower exponential decay taking place over tens of picoseconds. This can be assigned[28−30] to diffusive molecular rotational relaxation and can be examined quantitatively by fitting the OHD-OKE response beyond 1.5 ps to the sum of two exponential decays as

$$r_{\mathrm{diff}} = [a_1 \exp(-t/\tau_1) + a_2 \exp(-t/\tau_2)][1 - \exp(-2\omega_{\mathrm{av}}t)] \quad (1)$$

This function has been found to describe the picosecond dynamics of several liquids and solutions accurately.[28−30] The slower of the two relaxation times can often be ascribed to orientational diffusion. The shorter relaxation time is generally too fast to be attributed to molecular reorientation, but does, in general, appear to scale with the slower relaxation time. The results of fitting the data in Figure 3 to eq 1 are presented in Table 2.

The picosecond dynamics of all the 1 M concentration samples are well described by eq 1. Those in methanol showed a short decay time scale of 1.17 ± 0.05 ps and a longer decay ranging from 5.4 ps for phenol to 8.2 ps for hydroquinone. In acetonitrile, the shorter decay was 1.4 ± 0.15 ps while the longer one ranged from 4.2 to 6.7 ps, again in phenol and hydroquinone, respectively. It is apparent that the rotational time scale of each of the phenol derivatives is slower when dissolved in methanol than in acetonitrile. This can be ascribed to the greater viscosity of the solvent, which in turn is due to the increased hydrogen bonding that is present in methanol. This effect is observed clearly by the almost 3-fold increase in the rotational decay time scale of neat methanol over neat acetonitrile, a result that is in good agreement with previous studies.[36,56] Rotational diffusive motion of binary mixtures can often be well described by the Debye−Stokes−Einstein relation,

$$\tau_2 \approx \frac{g_2 V \eta}{k_{\mathrm{B}} T} \quad (2)$$

in which $\tau_2$ is the collective reorientation time measured by OHD-OKE (and other Raman techniques), $g_2$ is the static orientational pair correlation parameter, which scales between the collective and single molecule relaxation times (as measured by NMR, for example), and $V$ is the hydrodynamic volume.[57,58] In the case of acetonitrile and methanol, the slightly larger size of the former and the slightly larger viscosity of the latter suggest that similar rotational relaxation times would be expected. The observed difference is therefore due to the extra hydrogen bonding present in methanol.

As the rotational diffusion time scales of the neat solvents are shorter than those of the solutions it is reasonable to assume that $\tau_2$ of the solutions is largely due to the solute. The rotational times of the individual phenol derivatives, though similar, scale as $\tau_{\mathrm{phenol}} < \tau_{\mathrm{pyrocatechol}} < \tau_{\mathrm{hydroquinone}}$ which can be rationalized in terms of molecular shape—the longer, para-substitued, hydroquinone exhibiting slightly more hindered rotational behavior than the more compact pyrocatechol and smaller phenol.

When small quantities of methanol (up to 2 M) were added to hydroquinone in acetonitrile, the time-domain response was changed little although a small increase in $\tau_2$ was observed within the errors of the measurement, which appears to scale with methanol concentration.

**c. OHD-OKE Results: Frequency Domain.** As mentioned above, to discuss the dynamics of these samples more fully, it is desirable to transform the data to the frequency domain. A detailed description of the Fourier transform deconvolution procedure employed here can be found elsewhere.[30,31] Put simply, the Raman spectral density, undistorted by the finite instrument response time, is obtained from the imaginary part of the ratio of the Fourier transform of the OHD-OKE data to that of the second-order autocorrelation of the laser pulse. To focus on the ultrafast dynamics, the reduced spectral density can be obtained by first subtracting from the data that portion fit by eq 1. In this case, the procedure yields just the portion of the Raman spectral density attributable to nondiffusive motion, for example, librational and intermolecular (interaction-induced) relaxation. The justification for this procedure is the assumed time scale separation between ultrafast and diffusive dynamics. Since this assumption is somewhat questionable, at least in the case of the shorter exponential relaxation time, we present here both complete and reduced spectral densities. These are displayed in Figure 4.

A sharp spike at low frequency dominates the complete spectral densities of the six 1 M samples (Figure 4), which is due to the rotational diffusive dynamics. In all cases, the broad band below 150 $\mathrm{cm}^{-1}$ that is assignable to librational motion[59] is clearly observed. That the amplitude of the spectral densities of the acetonitrile samples is greater than those of the methanol

**TABLE 2: Results of Fitting Time-Domain OHD-OKE Data at Pump−Probe Delays Larger than 1.5 ps to Eq 1**[a]

| sample | $a_1$ | $\tau_1$ (ps) | $a_2$ | $\tau_2$ (ps) |
|---|---|---|---|---|
| methanol | | | | |
| neat | 0.0207 | 0.831 | 0.0056 | 5.025 |
| phenol | 0.0512 | 1.142 | 0.0276 | 5.399 |
| hydroquinone | 0.0307 | 1.207 | 0.0152 | 8.243 |
| pyrocatechol | 0.046 | 1.205 | 0.028 | 7.56 |
| acetonitrile | | | | |
| neat | 0.121 | 0.9365 | 0.1106 | 1.866 |
| phenol | 0.121 | 1.269 | 0.049 | 4.24 |
| hydroquinone | 0.1275 | 1.4508 | 0.0275 | 6.708 |
| pyrocatechol | 0.14 | 1.515 | 0.0427 | 6.27 |
| hydroquinone(MeOH)$_n$ | | | | |
| $n = 0.5$ | 0.133 | 1.42 | 0.031 | 6.89 |
| $n = 1$ | 0.123 | 1.41 | 0.033 | 7.00 |
| $n = 2$ | 0.126 | 1.40 | 0.033 | 7.05 |

[a] The samples are methanol and solutions in methanol; acetonitrile and solutions in acetonitrile; and solutions of hydroquinone in acetonitrile with the addition of 0.5, 1, and 2 M methanol. The viscosities of the solvents are[65] $\eta_{\mathrm{MeOH}} = 0.547$ cP at 298 K and $\eta_{\mathrm{acetonitrile}} = 0.345$ cP at 298 K.

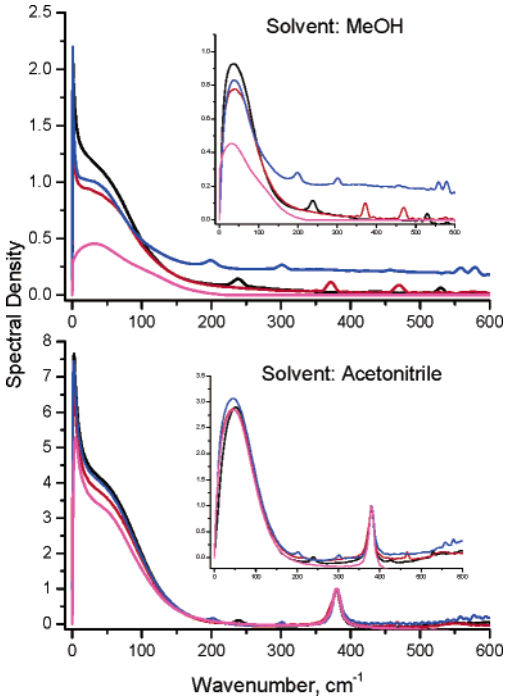


**Figure 4.** Complete and reduced (inset) spectral densities of 1 M solutions of phenol (black), hydroquinone (red), and pyrocatechol (blue). Complete spectral densities of the neat solvents are also shown (pink).

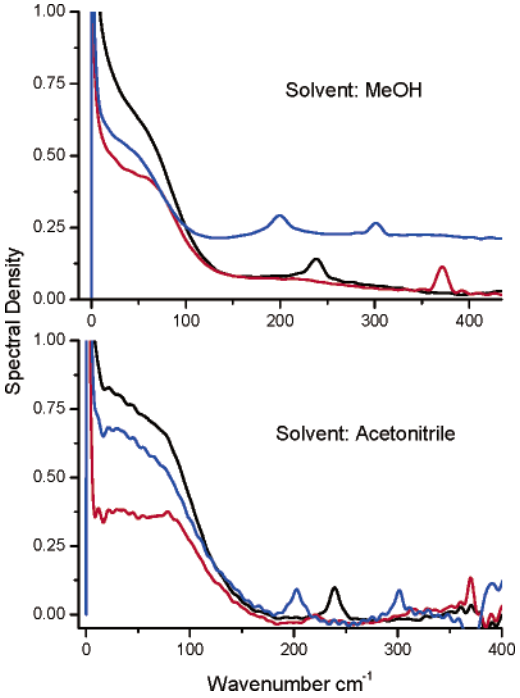


**Figure 5.** Solvent subtracted spectral densities of 1 M solutions of phenol (black), hydroquinone (red), and pyrocatechol (blue).

samples is again due to the larger polarizability of the solvent. The contribution of the phenol derivatives is approximately equal in each case because all samples are of the same concentration. Observable at frequencies in excess of 200 $cm^{-1}$ are low amplitude, narrow bands due to intramolecular vibrations of the solute (except that at 380 $cm^{-1}$ in the acetonitrile samples which is due to the solvent). Both the librational line shape and the intramolecular modes are more clearly observed in the tail-subtracted spectral densities (Figure 4, insets).

The spectral densities of the methanol solutions containing either phenol or hydroquinone show an additional contribution between 150 and 300 $cm^{-1}$. That of pyrocatechol shows a broadband offset of the baseline that persists to beyond the scope of the spectrometer at frequencies above 700 $cm^{-1}$ (the latter feature is both repeatable and scales with pyrocatechol concentration). Neither of these features is present in the acetonitrile samples.

As mentioned above, both of the solvents used exhibit nonzero OHD-OKE responses and it is therefore instructive to subtract the solvent response to ensure that these features are not due to the solvent background. In the case of acetonitrile, this was achieved by normalizing all spectral densities to the solvent intramolecular mode at 380 $cm^{-1}$ prior to subtracting the contribution due to the neat solvent. In the case of methanol, this approach was not possible but methanol has a significantly weaker OHD-OKE response than acetonitrile and so the neat solvent spectral density was simply subtracted with no prior weighting. The results of this process for the complete spectral densities are shown in Figure 5. It is clear from the figure that these features are not solvent related. In systems such as these where solvent−solute interactions are strong such a subtraction is not necessarily valid, and as such it will not be used in any subsequent analysis and is presented simply as a means to emphasize the effect being reported.

The additional amplitude in the spectral densities between 150 and 300 $cm^{-1}$ in the phenol and hydroquinone in methanol samples is apparently due to some interaction between the solvent and the solute (as is the broadband contribution to the

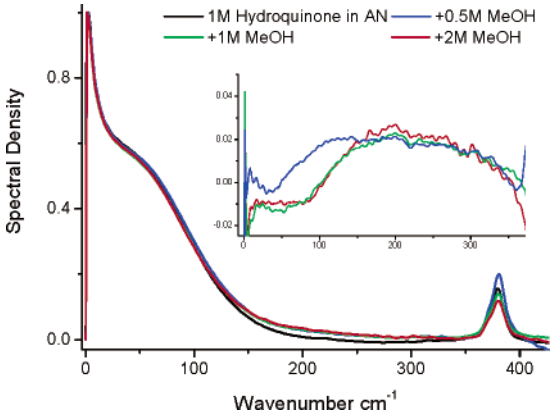


**Figure 6.** Spectral densities of 1 M hydroquinone dissolved in acetonitrile with 0 (black), 0.5 (blue), 1 (green), and 2 M (red) methanol added. The inset shows the result of subtracting the neat acetonitrile spectral density from that of each of the solutions.

pyrocatechol spectrum, which will be discussed in more detail below). It is instructive to study the dependence of the effect on methanol concentration. This is shown in Figure 6 where methanol was added to concentrations of 0.5, 1, and 2 M to a 1 M solution of hydroquinone in acetonitrile. Hydroquinone was chosen for this experiment because it features no strong intramolecular modes in the region of interest thereby greatly simplifying any observations. All spectra were normalized to the sharp, low-frequency rotational-diffusion feature although similar results were achieved by normalizing to the acetonitrile intramolecular mode and subsequent subtraction of the solvent response. The latter approach was prone to some distortion of the data due to the presence of an intramolecular mode of hydroquinone at 375 $cm^{-1}$. As can be clearly seen, the broad component between 150 and 300 $cm^{-1}$ persists for all methanol concentrations studied. This result shows that the addition of even small amounts of methanol leads to a modification of the spectral density of hydroquinone in this frequency region that can only be ascribed to solvent−solute interaction.

**d. Librational and Intermolecular Dynamics.** For further analyses, it is advantageous to separate the Raman spectral densities into two regions at this stage. The high-frequency (>300 $cm^{-1}$) portion, which is dominated by intramolecular vibrational modes, will be discussed in a separate subsection. Presented below is a more quantitative analysis of the low-frequency portion, which is dominated by librational motions and intermolecular interactions.

The broad and somewhat featureless nature of the low-frequency spectral density of most liquids means that fitting of the data is, to a certain extent, an arbitrary process. Some groups fit to a set of Brownian oscillators[27,47,60−62] while others claim that the sum of anti-symmetrized Gaussian line shapes with an Ohmic or Bucaro−Litovitz[30] type line shape gives superior results. In this work, the spectral densities of the 1 M solutions of phenol and hydroquinone in methanol and phenol, hydroquinone, and pyrocatechol in acetonitrile were fit to the sum of a Bucaro−Litovitz function

$$I_{BL}(\omega) = a_{BL}\omega^{\alpha}\exp(-\omega/\omega_{BL}) \quad (3)$$

and a set of anti-symmetrized Gaussian (ASG) profiles, defined by

$$I_G(\omega) = a_G\left[\exp\left(\frac{-2(\omega-\omega_G)^2}{\sigma_G^2(2\ln 2)^{-1}}\right) - \exp\left(\frac{-2(\omega+\omega_G)^2}{\sigma_G^2(2\ln 2)^{-1}}\right)\right] \quad (4)$$

**TABLE 3: Results of Fitting Spectral Densities of 1 M Solutions to Eqs 3 and 4**

| | methanol | | | acetonitrile | | | |
|---|---|---|---|---|---|---|---|
| | neat | phenol | hydroquinone | neat | phenol | hydroquinone | pyrocatechol |
| $a_{BL}$ | 0.01 | 0.05 | 0.07 | 0.09 | 0.06 | 0.04 | 0.03 |
| $\alpha$ | 1.39 | 1.27 | 1.09 | 1.08 | 1.10 | 1.28 | 1.36 |
| $\omega_{BL}$ ($cm^{-1}$) | 9.4 | 11.6 | 13.6 | 14.5 | 13.1 | 11.8 | 11.7 |
| $a_{G1}$ | 0.26 | 1.01 | 1.16 | 1.96 | 1.23 | 1.15 | 1.21 |
| $\omega_{G1}$ ($cm^{-1}$) | 28.0 | 32.9 | 31.1 | 32.0 | 36.3 | 40.1 | 36.5 |
| $\sigma_{G1}$ ($cm^{-1}$) | 68.3 | 109.0 | 116.8 | 119.8 | 119.0 | 117.9 | 120.0 |
| $a_{G2}$ | 0.23 | 0.09 | 0.16 | | | | |
| $\omega_{G2}$ ($cm^{-1}$) | 81.0 | 106.7 | 80.0 | | | | |
| $\sigma_{G2}$ ($cm^{-1}$) | 117.7 | 273.0 | 275.0 | | | | |
| $a_{G3}$ | - | 0.06[a] | | | 0.03[a] | | 0.027[a] |
| $\omega_{G3}$ ($cm^{-1}$) | - | 238.3[a] | | | 238.3[a] | | 200.8[a] |
| $\sigma_{G3}$ ($cm^{-1}$) | - | 17.2[a] | | | 17.9[a] | | 17.2[a] |

[a] Intramolecular mode.

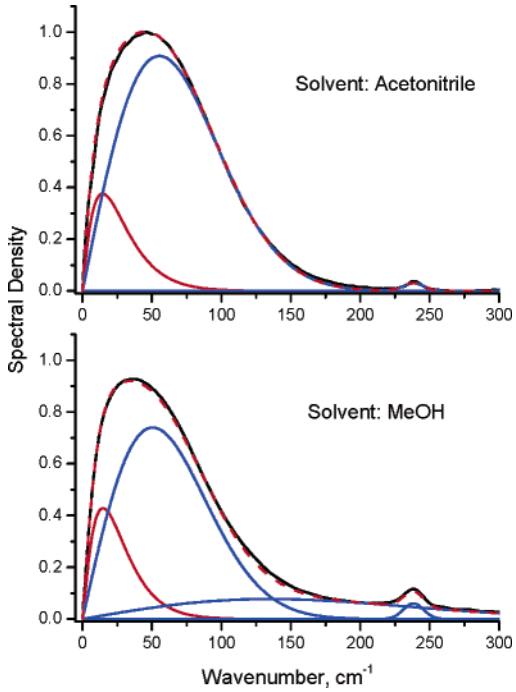


**Figure 7.** Fits (red dashed line) to reduced spectral densities (black line) of phenol dissolved in methanol and acetonitrile. Solid red lines show the component due to eq 3 and blue lines those due to eq 4.

Fits to the sum of a Lorentzian line shape and a suite of Brownian oscillators were also attempted but this approach required a greater number of Brownian oscillators than ASG functions to achieve the same quality of fit. In all cases, the spectral density with the rotational tail subtracted but without solvent subtraction was used for the fit. This approach removes the need for an additional function to fit the rotational dynamics and ensures that no artifacts from the solvent subtraction complicate the fitting process. Furthermore, the solvent subtraction approach assumes separability of the solvent and solute responses. This is not necessarily valid when considering solutions that exhibit strong solvent−solute interactions and it is thus more rigorous to consider the spectral density as a whole. The spectra obtained for pyrocatechol in methanol were not included in the fit due to the anomalous background component in the spectral density.

Table 3 shows the results of the fits to eqs 3 and 4 and Figure 7 displays example fits for phenol dissolved in methanol and acetonitrile. From the results it is clear that all of the spectral densities can be fit by a similar range of functions: the broad line shape at low frequency is well described by a Bucaro−Litovitz line shape with $\omega_{BL} = 11 \pm 2$ $cm^{-1}$ and one ASG line shape centered at $35 \pm 5$ $cm^{-1}$ with a width parameter ($\sigma_G$) of around 115 $cm^{-1}$. In addition, the samples in methanol require a second ASG function with $\omega \sim 90$ $cm^{-1}$ and $\sigma_G \sim 275$ $cm^{-1}$. As a result of the similarity of the width and spectral range, the standard deviation of this second ASG function is in the region of $\pm 40$ $cm^{-1}$. Phenol and pyrocatechol also require a narrow ASG profile to account for a low-lying intramolecular vibrational mode.

It is noteworthy that the neat solvents are themselves also fit by a similar range of functions (see Table 3). However, as is conclusively shown in Figure 5, the extra component found in the methanol solutions of phenol derivatives is not solely due to the solvent. This result merely serves to accentuate the similarity of the low-frequency spectral densities of many liquid samples.

**e. Intramolecular Vibrational Modes and DFT Calculations.** Despite the mid-infrared spectra of phenol, hydroquinone, and pyrocatechol being much studied[48−52] and well understood, some confusion still exists at low frequencies. While agreement seems to have been reached in the cases of phenol and hydroquinone, assignment of the low-frequency modes of pyrocatechol remains unclear. One of the major complicating factors is the state dependence of infrared and Raman transitions with shifts of tens of wavenumbers being observed between liquid and solid phases.[49] To establish fully any effects of hydrogen bonding on the low-frequency Raman spectral densities recovered here, it was first necessary to obtain a complete assignment of all observed bands. See Table 4 for complete lists of all observed bands and their assignments.

It is noteworthy that none of the modes showed a significant solvent dependence. In the cases of phenol and hydroquinone, assignment was relatively straightforward with use of existing studies.[49,52] For pyrocatechol, however, specific problems existed that related to the observed modes at 289 and 301 $cm^{-1}$. These appeared not to agree, even closely, with previous studies.[52] It seemed that the two modes were probably due to the symmetric out-of-plane and in-plane bending modes of the two hydroxyl groups; however, the latter was predicted to be Raman inactive while the former had not been previously assigned.

To solve this problem, DFT calculations of the equilibrium structure and vibrational modes of phenol, hydroquinone, and pyrocatechol were performed. The equilibrium structures are as shown in Chart 1 while the intramolecular modes and their assignments are listed in Table 4. The fact that the phenol and hydroquinone assignments were well established indicates the

**TABLE 4: Position and Assignments of Intramolecular Vibrational Bands of Phenol Derivatives**

| assignment[a] | Gaussian03/cm$^{-1}$ | Raman/cm$^{-1}$ | FIR/cm$^{-1}$ |
|---|---|---|---|
| phenol | | | |
| subs oop bend | 228 | 238 | 255 |
| O−H torsion | 310 | | |
| subs ip bend | 405 | 433 | 417 |
| asym ring def | 417 | | 452 |
| ring def | 509 | 508 | 509 |
| ring subs ip bend | 536 | 529 | 531 |
| hydroquinone | | | |
| subs sym oop bend | 153 | 219 | 200 |
| O−H asym torsion | 247 | | |
| O−H sym torsion | 261 | | |
| subs sym ip bend | 341 | 316 | |
| subs asym oop bend | 361 | 371 | |
| ring H oop bend | 420 | | |
| subs asym ip bend | 447 | 392 | 400 |
| sym ring def | 471 | 467 | 470 |
| pyrocatechol | | | |
| O−H torsion, no H bond | 146 | | |
| subs oop asym bend | 190 | 199 | |
| subs oop sym bend | 292 | 289 | |
| subs ip sym bend | 309 | 301 | |
| O−H torsion, H bond | 414 | | |
| subs ip assym bend | 448 | 456 | 456 |
| ring H oop bend | 451 | 456 | |
| ring subs ip bend | 559 | 558 | 559 |

[a] "Subs" indicates substituent or hydroxyl groups, oop and ip indicate and out-of-plane and in-plane motion, respectively.

accuracy of the calculations. From Table 4, it is clear that the agreement for phenol is impressive with accuracy generally better than $\pm 5$ cm$^{-1}$ even though the calculations were performed on gas-phase molecules. One exception is the O−H group in-plane bend of phenol, observed here at 433 cm$^{-1}$ and predicted at 405 cm$^{-1}$. This mode could also be assignable to the ring deformation mode predicted at 417 cm$^{-1}$. However, the calculations indicate that the latter is both IR and Raman inactive, hence the assignment given in Table 4.

The results for hydroquinone, while not displaying the same impressive accuracy as those for phenol, are still generally accurate to $\pm 30$ cm$^{-1}$. The discrepancies can be attributed to solvent−solute interactions not accounted for when using DFT methods. The case of the OH group asymmetric in-plane bend of hydroquinone is worthy of note. Predicted at 447 cm$^{-1}$ it is assigned to the mode observed at 392 cm$^{-1}$ despite the fact that the ring hydrogen out-of-plane bend is predicted to lie closer in frequency at 420 cm$^{-1}$. The latter, however, is calculated to be both IR and Raman inactive hence the assignment given in Table 4.

In the case of pyrocatechol, the agreement with experiment is also very good, to the extent that a complete assignment of the low-frequency modes has been possible for the first time. It is also apparent that the symmetric and asymmetric in-plane bends, predicted to be Raman inactive,[52] are in fact weakly visible. This is due to the presence of the intramolecular hydrogen bond in the equilibrium structure of pyrocatechol, which lowers the symmetry of the molecule and which was apparently neglected in previous studies.

Hydrogen torsional modes are predicted by the DFT calculations for all three phenol derivatives but not observed. These modes are due to rotation about the C−OH bond and as such would be expected to generate little change in the polarizability of the molecule with vibrational coordinate and thus be weakly Raman-active at best. The calculations predict, however, that they should be of similar intensity to the observed intramolecular modes. A possible reason for these modes not being observed may lie in the fact that they are also predicted to have large transition dipole moments. As such they will couple strongly to the polar solvent bath and be strongly damped in the solution phase, which is not accounted for in the gas-phase calculations.

It is interesting to compare the frequencies of these modes in the different phenol derivatives. In phenol, the single OH torsional mode is predicted to occur at 310 cm$^{-1}$ while in hydroquinone two modes appear close to 250 cm$^{-1}$. In contrast, the corresponding modes of pyrocatechol are calculated to lie at 146 and 414 cm$^{-1}$, the latter being assigned for the hydrogen atom directly involved in the intramolecular H-bond. This indicates that the intramolecular hydrogen bond is of appreciable strength, which raises the energy change associated with vibrational motion and increases the frequency.

Far-infrared (FIR) spectroscopy of the solutions of the phenol derivatives in methanol has also been undertaken. Due to the strong solvent absorption in this region, it was necessary to use much higher concentrations of solute than for the OHD-OKE studies; as such, far-IR spectra of the acetonitrile solutions were not possible because the phenols are less soluble in this solvent than in methanol. However, little solvent dependence of the Raman active modes was observed and consequently little frequency variation was expected in the far-IR case. Table 4 lists the far-infrared modes observed and there is good agreement between the far-infrared spectra, Raman spectral density, and DFT calculations. Once again, the O−H torsional modes were not observed despite being predicted to possess a large IR intensity; this may be due to the strong solvent background at very low frequencies. However, a ring deformation mode of phenol at 452 cm$^{-1}$ not present in the Raman spectrum was observed. This is in agreement with the DFT calculations, which show this mode to be IR active only.

Finally, it is instructive to consider the line width of the observed modes in both Raman and FTIR spectra. While those assigned to librational motion, observed at very low frequency ($<150$ cm$^{-1}$), are very broad, the transitions due to intramolecular modes are invariably much narrower ($\sim 20$ cm$^{-1}$). This can be explained by the greater damping of librational modes due to the larger amount of solvent displacement associated with the motion. It is interesting to note, however, that the modes directly associated with the intramolecular hydrogen bond of pyrocatechol, i.e., those involving in-plane or out-of-plane motion of the substituent groups, are not broadened in the manner of the O−H stretching and intermolecular H-bond modes. As this effect is attributed to inhomogeneous broadening due to a range of solvent−solute environments this would appear to suggest that this is not the case for the intramolecular mode, further indicating the relative strength of this bond. It would also seem reasonable to suggest that this bond lacks the dynamic nature of its solvent−solute counterpart.

**f. Poly-L-Tyrosine.** Figure 8 shows the OHD-OKE response of poly-L-tyrosine (PLT) dissolved in water and in methanol. In both cases, sodium hydroxide was added to a concentration of 100 mM to facilitate PLT solubility. The PLT concentration was $\sim 20$ mg/mL in water and approximately twice that in

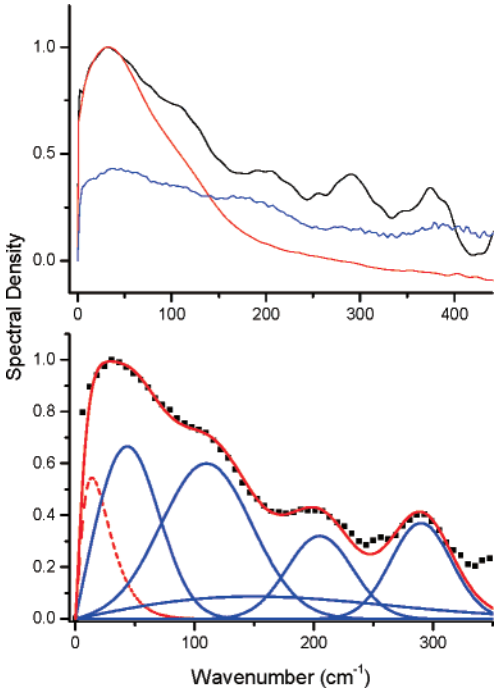


**Figure 8.** Top: Complete (non-solvent-subtracted) spectral densities of PLT dissolved in basic solutions of methanol (black line) and water (blue). The red line shows the complete spectral density of methanol. Bottom: Comparison of experimental (black dots) and simulated (solid red line) spectral density of PLT dissolved in methanol using eq 3 (red dashed line) and five ASG functions (eq 4, solid blue lines).

methanol. In both cases, this was approaching a saturated solution.

Due to the low concentrations of PLT (these weight percentages equate to approximately 125−250 mM in terms of amino acid residues), the time-domain OHD-OKE traces (not shown) appear largely indistinguishable from those of the solvent; however, the complete spectral densities of the PLT solutions exhibit clear contributions from the polypeptide. In the basic solutions used, PLT has been shown by vibrational circular dichroism studies to assume a random coil rather than α-helical structure.[63] Previous studies of polymers with large side groups[33] have shown a tendency for a shift away from long rotational relaxation time scales toward relaxation through low-frequency intramolecular modes with increasing chain length. These observations appear to hold for PLT (mol wt ∼10−40 000), which shows no apparent slow rotational decay but exhibits many low-frequency vibrational modes.

It is also noteworthy that, when dissolved in methanol, the PLT Raman spectral density displays nonzero amplitude between 150 and 300 $cm^{-1}$ similar to that of the model systems discussed above. While a convolution of low-frequency modes could cause this effect it seems likely—in light of earlier results—that solvent−solute interactions between methanol and the phenol side groups of the PLT chain are also at least partially responsible. This qualitative assessment is further supported by fitting the PLT spectral density using eqs 3 and 4. The result is shown in Figure 8. In this case, five ASG functions were required to accurately reproduce the spectral density of PLT in methanol, one of which was centered at 120 $cm^{-1}$ with a large width of $\sigma_G = 300$ $cm^{-1}$, similar to the results obtained for the model systems above. The other ASG functions were centered at 43, 110, 205, and 290 $cm^{-1}$ with $\sigma_G$ values of ∼60 $cm^{-1}$ except for the 110 $cm^{-1}$ mode, which was broader ($\sigma_G = 90$ $cm^{-1}$). Attempts to reproduce the experimental data without the broad extra component were unsuccessful. The mode at 370 $cm^{-1}$ has not been included in the fit. Due to the low concentration of PLT in this sample the results of the Fourier transform technique become noisy and the line shapes distorted at these frequencies.

Though very complex, it is possible to assign some parts of the PLT low-frequency spectrum by analogy with previous work. The band close to 50 $cm^{-1}$ is analogous to that observed in the model systems above and can be attributed to librational motion of the phenol side groups. The prominent shoulder at around 110 $cm^{-1}$ is similar to that reported in a recent study of polystyrene.[33] In that case, it was assigned to torsional motion of the phenyl side groups about the polymer backbone, an assignment that would also be applicable in this case.

Further, the mode centered at 205 $cm^{-1}$ can be assigned to the out-of-plane bend of the phenol hydroxyl group by direct analogy with the experimental and theoretical studies above. That this mode is broadened and slightly shifted from that of phenol can be attributed to the large molecular weight of the polymer leading to inhomogeneous broadening of this band. In a similar fashion, the modes close to 400 $cm^{-1}$ may be due to the hydroxyl group in-plane bend, but this can only be tentatively suggested without detailed simulations, which are difficult and computationally expensive. Simulations of this nature are planned for a future study.

## IV. Discussion

It is important to consider the nature of the molecular systems being studied. At the concentrations used the solvent-to-solute molecular ratio is 25:1 in methanol and 20:1 in acetonitrile, and it is thus possible that phenol−phenol interactions are present in these samples, in addition to phenol−methanol interactions, leading to dimer or cluster formation. These cannot, however, be responsible for the additional feature observed in the spectral densities of the methanol solutions because such clusters would be expected to form in the acetonitrile solutions also and the corresponding feature was absent in the spectra of these solutions. Indeed such an effect would be expected to be larger in acetonitrile solutions due to the reduced solvent−solute interactions compared to those in methanol.

As mentioned above, studies have been carried out on gas-phase clusters of the type phenol$(methanol)_n$ in supersonic jets containing mixtures of phenol and methanol.[2] A broad background feature superimposed upon lines assigned to the phenol-$(MeOH)_1$ cluster was reported in the laser-induced fluorescence spectrum.[2] This was attributed to the inhomogeneous spectral congestion caused by the existence of different cluster sizes and isomers in the jet. This feature is very similar to the broad feature observed with our data and it seems reasonable to suggest that this is in fact the high methanol concentration (large $n$) limit for the clusters, or the signature of hydrogen bonding between phenol and the bulk liquid. The fact that it is a broad feature is analogous to the breadth observed in the phenol OH stretching vibration by FTIR above, indicating the dynamic nature of intermolecular hydrogen bonds.

This assignment has important implications for the study of low-frequency modes in liquid systems in which hydrogen bonding occurs. From neat water and methanol, to the phenol derivative model systems discussed here, and polypeptides such as PLT this feature is observed. Furthermore, OHD-OKE studies of aqueous solutions of di-L-alanine, poly-L-alanine, α-lactalbumin, $\beta$-lactoglobulin, lysozyme, and pepsin show that a similar feature was observed in all of the low-frequency Raman spectral densities of these systems, even after careful subtraction of the water background spectrum.[47]

The broadband contribution to the spectrum of pyrocatechol in methanol has not been discussed in any detail so far. While in no way contradictory to the above results, it is certainly anomalous and the explanation unclear. As it appears only in the spectrum of pyrocatechol dissolved in methanol it would appear to be due to some kind of interaction between the solvent and solute; however, it is markedly different from what is observed in the cases of phenol and hydroquinone. The fact that the feature extends to such high frequencies would seem to rule out an assignment solely to inter- and intramolecular H-bonds.

Studies have shown that the feature scales with pyrocatechol concentration, which rules out an experimental artifact. Similar broad background features have been observed in studies of polymers[64] and assigned to vibrational modes of the bulk polymer. However, this assignment seems somewhat unlikely in this case, unless, despite careful countermeasures some light degradation of the sample has occurred leading to polymerization or that pyrocatechol forms clusters/chains in solution. The former is unlikely because the spectrum of the pyrocatechol in methanol samples was not observed to change over time. The latter seems unlikely for two reasons, first that such behavior is not observed in the other phenol derivatives and second that any such effect would also occur in acetonitrile—this was not observed. This sample is the subject of ongoing study including simulations with instantaneous normal-mode methods, which will be the topic of a forthcoming publication.

As mentioned above, there have been many indirect studies of hydrogen-bonded systems using mid-infrared absorption spectroscopy of the OH or OD stretching vibrations. The work of Rezus et al.[12] in particular used mid-infrared femtosecond pump−probe spectroscopy to study phenol-*d* dissolved in chloroform and acetone. In that work a 3.7 ps decay time scale observed in the anisotropy of the transient absorption was reported which was subsequently assigned to nutation of the OD group about the C−O axis in conjunction with a longer decay time (>30 ps) being observed when excitation on the red side of the OD absorption profile was performed. In light of the results of this study, however, this assignment seems unlikely as the molecular rotational diffusion time for phenol solutions in methanol was observed to be ∼5 ps. This suggests that the nutation time of the OD group would be expected to be faster than 3.7 ps. In addition, no long time scale components were observed out to 50 ps.

## V. Conclusions

OHD-OKE studies have been carried out on a variety of solutions of phenol derivatives in methanol and acetonitrile. FTIR spectroscopy has been used to show that solutions involving the former feature significantly stronger solvent−solute hydrogen bonding than the latter. Analysis of the Raman spectral density of these solutions has shown that an extra component appears in the methanol samples that is not present when acetonitrile is the solvent. This feature is a broad line shape centered at around 100 $cm^{-1}$ and is analogous to that observed in gas-phase studies of phenol(methanol)$_n$ clusters for large *n*. It is assigned to an inhomogeneously broadened transition due to solvent−solute intermolecular hydrogen bonds.

The studies of phenol derivatives have been used as a model system for an OHD-OKE study of poly-L-tyrosine. The low-frequency Raman spectral density of this species dissolved in methanol and water also shows a similar feature, as have previous studies of other polypeptide and protein-based systems.[47]

The low-frequency intramolecular modes of phenol, hydroquinone, and pyrocatechol have been assigned, the latter for the first time, with the aid of DFT calculations. It has been shown that the equilibrium structure of pyrocatechol features an intramolecular hydrogen bond, which significantly influences the low-frequency vibrational Raman spectrum.

**Acknowledgment.** The authors acknowledge funding for this project from the Engineering and Physical Sciences Research Council (EPSRC) and the Leverhulme Trust.

## References and Notes

(1) Tanabe, S.; Ebata, T.; Fujii, M.; Mikami, N. *Chem. Phys. Lett.* **1993**, *215*, 347.
(2) Schmitt, M.; Muller, H.; Henrichs, U.; Gerhards, M.; Perl, W.; Deusen, C.; Kleinermanns, K. *J. Chem. Phys.* **1995**, *103*, 584.
(3) Schiefke, A.; Deusen, C.; Jacoby, C.; Gerhards, M.; Schmitt, M.; Kleinermanns, K.; Hering, P. *J. Chem. Phys.* **1995**, *102*, 9197.
(4) Schmitt, M.; Jacoby, C.; Gerhards, M.; Unterberg, C.; Roth, W.; Kleinermanns, K. *J. Chem. Phys.* **2000**, *113*.
(5) Lim, M.; Hochstrasser, R. M. *J. Chem. Phys.* **2001**, *115*, 7629.
(6) Deak, J. C.; Rhea, S. T.; Iwaki, L. K.; Dlott, D. D. *J. Phys. Chem. A* **2000**, *104*, 4866.
(7) Huse, N.; Heyne, K.; Dreyer, J.; Nibbering, E. T. J.; Elsaesser, T. *Phys. Rev. Lett.* **2003**, *91*, 197401.
(8) Pakoulev, A.; Wang, Z.; Pang, Y.; Dlott, D. D. *Chem. Phys. Lett.* **2003**, *380*.
(9) Fecko, C. J.; Eaves, J. D.; Loparo, J. J.; Tokmakoff, A.; Geissler, P. L. *Science* **2003**, *301*, 1698.
(10) Gale, G. M.; Gallot, G.; Hache, F.; Lascoux, N.; Bratos, S.; Leicknam, J.-C. *Phys. Rev. Lett.* **1999**, *80*, 2622.
(11) Laenen, R.; Rauscher, C.; Lauberau, A. *Phys. Rev. Lett.* **1998**, *80*, 2622.
(12) Rezus, Y. L. A.; Madsen, D.; Bakker, H. J. *J. Chem. Phys.* **2004**, *121*, 10599.
(13) Ginn, S. G. W.; Wood, J. L. *Spectrochim. Acta* **1967**, *23A*, 611.
(14) Parthasarathi, R.; Subramanian, V.; Sathyamurthy, N. *J. Phys. Chem. A* **2005**, *109*, 843.
(15) Dimitrova, Y. *J. Mol. Struct.* (*THEOCHEM*) **2000**, *499*, 207.
(16) Bandyopadhyay, I.; Lee, H. M.; Kim, K. S. *J. Phys. Chem. A* **2005**, *109*, 1720.
(17) McMorrow, D.; Lotshaw, W. T. *J. Phys. Chem.* **1991**, *95*, 10395.
(18) Lotshaw, W. T.; McMorrow, D.; Kenney-Wallace, G. A. *Proc. SPIE* **1988**, *981*, 20.
(19) Back, R.; Kenneywallace, G. A.; Lotshaw, W. T.; McMorrow, D. *Chem. Phys. Lett.* **1992**, *191*, 423.
(20) McMorrow, D.; Lotshaw, W. T. *Chem. Phys. Lett.* **1993**, *201*, 369.
(21) McMorrow, D.; Lotshaw, W. T. *Chem. Phys. Lett.* **1990**, *174*, 85.
(22) McMorrow, D.; Lotshaw, W. T.; Kenneywallace, G. A. *IEEE J. Quantum Electron.* **1988**, *24*, 443.
(23) McMorrow, D.; Lotshaw, W. T. *Chem. Phys. Lett.* **1991**, *178*, 69.
(24) Palese, S.; Mukamel, S.; Miller, R. J. D.; Lotshaw, W. T. *J. Phys. Chem.* **1996**, *100*, 10380.
(25) McMorrow, D.; Thantu, N.; Melinger, J. S.; Kim, S. K.; Lotshaw, W. T. *J. Phys. Chem.* **1996**, *100*, 10389.
(26) Kalpouzos, C.; McMorrow, D.; Lotshaw, W. T.; Kenneywallace, G. A. *Chem. Phys. Lett.* **1988**, *150*, 138.
(27) McMorrow, D.; Thantu, N.; Kleiman, V.; Melinger, J. S.; Lotshaw, W. T. *J. Phys. Chem. A* **2001**, *105*, 7960.
(28) Lotshaw, W. T.; McMorrow, D.; Thantu, N.; Melinger, J. S.; Kitchenham, R. *J. Raman Spectrosc.* **1995**, *26*, 571.
(29) Kinoshita, S.; Kai, Y.; Ariyoshi, T.; Shimada, Y. *Int. J. Mod. Phys. B* **1996**, *10*, 1229.
(30) Smith, N. A.; Meech, S. R. *Int. Rev. Phys. Chem.* **2002**, *21*, 75.
(31) Hunt, N. T.; Jaye, A. A.; Meech, S. R. *J. Phys. Chem. B* **2003**, *107*, 3405.
(32) Hunt, N. T.; Jaye, A. A.; Meech, S. R. *Chem. Phys. Lett.* **2003**, *371*, 304.
(33) Hunt, N. T.; Jaye, A. A.; Hellman, A.; Meech, S. R. *J. Phys. Chem. B* **2004**, *108*, 100.
(34) Jaye, A. A.; Hunt, N. T.; Meech, S. R. *Langmuir* **2005**, *21*, 1238.
(35) Loughnane, B. J.; Farrer, R. A.; Scodinu, A.; Reilly, T.; Fourkas, J. T. *J. Phys. Chem. B* **2000**, *104*, 5421.
(36) Loughnane, B. J.; Farrer, R. A.; Scodinu, A.; Fourkas, J. T. *J. Chem. Phys.* **1999**, *111*, 5116.
(37) Farrer, R. A.; Loughnane, B. J.; Fourkas, J. T. *J. Phys. Chem. A* **1997**, *101*, 4005.
(38) Loughnane, B. J.; Fourkas, J. T. *J. Phys. Chem. B* **1998**, *102*, 10288.

(39) Gottke, S. D.; Brace, D. D.; Cang, H.; Bagchi, B.; Fayer, M. D. *J. Chem. Phys.* **2002**, *116*, 360.
(40) Gottke, S. D.; Cang, H.; Bagchi, B.; Fayer, M. D. *J. Chem. Phys.* **2002**, *116*, 6339.
(41) Hyun, B. R.; Quitevis, E. L. *Chem. Phys. Lett.* **2003**, *370*, 725.
(42) Hunt, N. T.; Meech, S. R. *J. Chem. Phys.* **2004**, *120*, 10828.
(43) Sengupta, A.; Terazima, M.; Fayer, M. D. *J. Phys. Chem.* **1992**, *96*, 8619.
(44) Sengupta, A.; Fayer, M. D. *J. Chem. Phys.* **1994**, *100*, 1673.
(45) Shirota, H.; Castner, E. W. *J. Am. Chem. Soc.* **2001**, *123*, 12877.
(46) Giraud, G.; Wynne, K. *J. Am. Chem. Soc.* **2002**, *124*, 12110.
(47) Giraud, G.; Karolin, J.; Wynne, K. *Biophys. J.* **2003**, *85*, 1903.
(48) Evans, J. C. *Spectrochim. Acta* **1960**, *16*, 1382.
(49) Tripathi, G. N. R. *J. Chem. Phys.* **1979**, *71*, 4025.
(50) Kubinyi, M. J.; Keresztury, G. *Mikrochim. Acta* **1997**, *14*, 525.
(51) Rao, R.; Sakuntala, T.; Arora, A. K.; Deb, S. K. *J. Chem. Phys.* **2004**, *121*, 7320.
(52) Varsanyi, G. *Assignments for Vibrational Spectra of 700 Benzene Derivatives*; Wiley: New York, 1974.
(53) Giraud, G.; Gordon, C. M.; Dunkin, I. R.; Wynne, K. *J. Chem. Phys.* **2003**, *119*, 464.
(54) Frisch, M. J.; Trucks, G. W.; Schlegel, H. B.; Scuseria, G. E.; Robb, M. A.; Cheeseman, J. R.; Montgomery, J. A., Jr.; Vreven, T.; Kudin, K. N.; Burant, J. C.; Millam, J. M.; Iyengar, S. S.; Tomasi, J.; Barone, V.; Mennucci, B.; Cossi, M.; Scalmani, G.; Rega, N.; Petersson, G. A.; Nakatsuji, H.; Hada, M.; Ehara, M.; Toyota, K.; Fukuda, R.; Hasegawa, J.; Ishida, M.; Nakajima, T.; Honda, Y.; Kitao, O.; Nakai, H.; Klene, M.; Li, X.; Knox, J. E.; Hratchian, H. P.; Cross, J. B.; Bakken, V.; Adamo, C.; Jaramillo, J.; Gomperts, R.; Stratmann, R. E.; Yazyev, O.; Austin, A. J.; Cammi, R.; Pomelli, C.; Ochterski, J. W.; Ayala, P. Y.; Morokuma, K.; Voth, G. A.; Salvador, P.; Dannenberg, J. J.; Zakrzewski, V. G.; Dapprich, S.; Daniels, A. D.; Strain, M. C.; Farkas, O.; Malick, D. K.; Rabuck, A. D.; Raghavachari, K.; Foresman, J. B.; Ortiz, J. V.; Cui, Q.; Baboul, A. G.; Clifford, S.; Cioslowski, J.; Stefanov, B. B.; Liu, G.; Liashenko, A.; Piskorz, P.; Komaromi, I.; Martin, R. L.; Fox, D. J.; Keith, T.; Al-Laham, M. A.; Peng, C. Y.; Nanayakkara, A.; Challacombe, M.; Gill, P. M. W.; Johnson, B.; Chen, W.; Wong, M. W.; Gonzalez, C.; Pople, J. A. *Gaussian 03*, revision C.01; Gaussian, Inc.: Wallingford, CT, 2004.
(55) Corcelli, S. A.; Lawrence, C. P.; Skinner, J. L. *J. Chem. Phys.* **2004**, *120*, 8107.
(56) Shirota, H.; Yoshihara, K.; Smith, N. A.; Lin, S. J.; Meech, S. R. *Chem. Phys. Lett.* **1997**, *281*, 27.
(57) Kivelson, D.; Madden, P. A. *Annu. Rev. Phys. Chem.* **1980**, *31*, 523.
(58) Berne, B. J.; Pecora, R. *Dynamic Light Scattering*; Wiley: New York, 1976.
(59) Smith, N. A.; Meech, S. R. *J. Phys. Chem. A* **2000**, *104*, 4223.
(60) Cho, M.; Du, N.; Scherer, N. F.; Fleming, G. R.; Mukamel, S. *J. Chem. Phys.* **1993**, *99*, 2410.
(61) Steffen, T.; Meinders, N.; Duppen, K. *J. Phys. Chem. A* **1998**, *102*, 4213.
(62) Steffen, T.; Fourkas, J. T.; Duppen, K. *J. Chem. Phys.* **1996**, *105*, 7364.
(63) Watanabe, K.; Muto, K.; Ishii, T. *Biospectroscopy* **1997**, *3*, 103.
(64) Hunt, N. T.; Meech, S. R. *Chem. Phys. Lett.* **2004**, *400*, 368.
(65) Weast, R. C. *CRC Handbook of Chemistry and Physics*; CRC Press: Cleveland OH, 1978.